Omics Assisted N-terminal Proteoform and Protein Expression Profiling On Methionine Aminopeptidase 1 (MetAP1) Deletion*[S]

Veronique Jonckheere‡§¶, Daria Fijałkowska‡§, and Petra Van Damme‡§¶‖

Excision of the N-terminal initiator methionine (iMet) residue from nascent peptide chains is an essential and omnipresent protein modification carried out by methionine aminopeptidases (MetAPs) that accounts for a major source of N-terminal proteoform diversity. Although MetAP2 is known to be implicated in processes such as angiogenesis and proliferation in mammals, the physiological role of MetAP1 is much less clear. In this report we studied the omics-wide effects of human MetAP1 deletion and general MetAP inhibition. The levels of iMet retention are inversely correlated with cellular proliferation rates. Further, despite the increased MetAP2 expression on MetAP1 deletion, MetAP2 was unable to restore processing of Met-Ser-, Met-Pro-, and Met-Ala- starting N termini as inferred from the iMet retention profiles observed, indicating a higher activity of MetAP1 over these N termini. Proteome and transcriptome expression profiling point to differential expression of proteins implicated in lipid metabolism, cytoskeleton organization, cell proliferation and protein synthesis upon perturbation of MetAP activity. ***Molecular & Cellular Proteomics 17: 10.1074/mcp.RA117.000360, 694–708, 2018.***

Protein biogenesis is one of the most fundamental and complex biological processes, with important implications for human health and disease. The concerted action of the ribosome and numerous ribosome-associated factors is essential to ensure proper initiation of translation, protein folding, processing and targeting. By the successive steps of ternary complex recruitment, ribosome scanning, start codon selection and ribosomal subunit joining, translation initiation acts as the gate-keeping step of translation. Here, protein biogenesis initiates with either an initiator N-formylmethionine (fMet)[1] in case of bacterial and eukaryotic organellar protein synthesis, or an initiator methionine (iMet) in case of archaeal and eukaryotic cytosolic protein synthesis.

Typically, for more than half of all nascent protein chains, the iMet is cotranslationally removed by the action of methionine aminopeptidases (MetAPs), a process referred to as N-terminal (Nt-) methionine excision (NME) (1). MetAPs represent a family of conserved and essential enzymes, as inferred from the lethality of the *map* null mutant in case of *Salmonella typhimurium* and *Escherichia coli* (2). Although typically only one MetAP gene is found in the genome of prokaryotes, eukaryotes express at least two types of cytosolic MetAPs belonging to a family of evolutionary conserved metalloproteases, being a type 1 and type 2 MetAP.

Although MetAP2 by itself was shown to be essential for the development of specific tissues in multicellular organisms (3), and MetAP1 appears to be vital for cell proliferation, a clear redundancy between MetAP1 and MetAP2 has been observed in *Arabidopsis thaliana* and *Saccharomyces cerevisiae*. Not surprisingly, double deletion mutants are nonviable, again pointing to their essential nature (4, 5). Further, and irrespective of their limited sequence identity, the catalytic domains of both MetAPs adopt a similar protein fold encompassing a highly conserved pocket for iMet binding (6, 7).

In case of eubacterial, mitochondrial and plastid NME, MetAPs remove the iMet of nascent polypeptide chains only after deformylation by the action of peptide deformylases (PDF) (8, 9). Further, the manifestation of (the extent of) iMet processing by MetAPs typically relates to the identity of the extreme N-terminal residues of the nascent polypeptide chain. More specifically, MetAPs only cleave iMet from nascent polypeptide chains in case of penultimate N-terminal residues (P1′) with (relatively) small and uncharged side

From the ‡VIB-UGent Center for Medical Biotechnology, B-9000 Ghent, Belgium; §Department of Biochemistry, Ghent University, B-9000 Ghent, Belgium

Received September 26, 2017, and in revised form, December 12, 2017

Published, MCP Papers in Press, January 9, 2018, DOI 10.1074/mcp.RA117.000360

Author contributions: P.V.D. designed research; P.V.D. performed research; P.V.D. analyzed data; P.V.D. wrote the paper; V.J. and P.V.D. performed experiments; D.F. analyzed transcriptome data.

[1] The abbreviations used are: fMet, N-formylmethionine; FDR, false discovery rate; iMet, initiator methionine; iBAQ, intensity based absolute quantification; LFQ, label free quantification; MetAP, methionine aminopeptidase; NAT, N-terminal acetyltransferase; NHEJ, nonhomologous end-joining; NME, N-terminal methionine excision; Nt, N-terminal; PDF, peptide deformylase; RPKM, reads per kilobase of exon per million fragments; SCX, strong cation exchange; SREBP, sterol regulatory element binding protein; TIS, translation initiation site.

chains (*i.e.* Gly, Ser, Ala, Pro, Cys, Thr, or Val) (10). The latter referred to as NME compatible residues. Furthermore, amino acid residues beyond P1′ may also contribute to the efficiency of NME (11–15). Interestingly and although still unclear, the need for having a MetAP of eubacterial and archaeal origin, being MetAP1 and MetAP2 respectively, might be attributed to (slight) differences in their substrate specificity profiles.

Further, the N-terminal amino acid sequence is also the major feature determining whether or not a given protein is Nt-acetylated and by which Nt-acetyltransferase or NAT (16). As such, the interplay among other co-translational acting modifiers, such as the NATs responsible for the cotranslational Nt-acetylation of a large cohort of proteins in case of eukaryotes (17–19), has also been implicated in determining MetAP susceptibility and thus (the extend of) iMet retention. More specifically we have previously shown Nt-acetylated iMet to be refractory toward the action of MetAPs (20).

By having different processing enzymes operating at the ribosomal exit tunnel, each nascent protein may undergo several cotranslational modifications before being fully matured.

Consequently, different N-terminal proteoforms might display characteristic functionalities, such as altered protein stabilities (21–23) and subcellular localization. Consequently, Nt-modifications contribute to the increase of protein complexity observed.

In this study, we studied the omics-wide effects of human MetAP1 deletion using a human haploid HAP1 MetAP1 knockout cell line model and compared it to general MetAP inhibition using Bengamide B, a marine-derived natural product with broad spectrum antitumor activity which functions as a nanomolar inhibitor of MetAPs 1 and 2 (24). The use of these different setups additionally enable discriminating more direct from indirect MetAP actions. By enriching for protein N termini using positional proteomics, we revealed the *in vivo* substrate profile of MetAP1 at the proteome-wide level, thereby aiding in elucidating the functional role of MetAPs. Furthermore, our proteome analysis showed that the increased expression of MetAP2 observed on MetAP1 deletion was unable to restore processing of MS-, MP- and MA- N termini, overall pointing to MetAP1 as the MetAP being exclusively or more active over these N termini and providing increasing knowledge on the *in vivo* substrate repertoire of MetAPs.

Only in specific cases of which the iMet-processed and iMet unprocessed Nt-proteoforms could be observed, iMet processing affected the steady-state Nt-acetylation levels of Nt-proteoforms. Interestingly, changes in steady-state protein expression levels were typically explained at the transcript level and not related to protein N-terminal amino acid identities. More specifically, upon perturbation of MetAP activity, omics expression profiling revealed differential expression of proteins implicated in lipid metabolism, cytoskeleton organization, cell proliferation and protein synthesis.

EXPERIMENTAL PROCEDURES

Cell Culture—HAP1 control cells (HAP1 WT) and CRISPR/Cas9 edited human METAP1 knockout cells (HAP1 MetAP1 KO) containing a frameshift mutation in a coding exon of METAP1 (*i.e.* HAP1 cells carrying a 179bp insertion 'ATACAGAGTGACATAATGGACACTANAGACTCANAGTGGGGAGGGTAAGAGGGGGGCAAGGNATAAAAAACCACATATTGGGTACAATGTACACTACTCAGGTGACCGGTGCAGTAAAATCTCANACTTCNCTACTGTAGAATTCATCTATATGACCAAAAGCCATTTGTACCCCAAAA' in exon 4 of NM_015143 at chr4: 99035439, leading to the corresponding MetAP1 genomic sequence of CAAAGACCAGAT(179 bp insertion)TATGCTGATCAT which was sequence verified by Sanger sequencing on PCR amplification from purified genomic DNA using the following primers; CTTTCTAAATACCCTGCAAAAGGGG (forward) and TCTTCAATGTTCTAATGGTGCTTG (reverse)) were obtained from Horizon Genomics GmbH (Vienna, Austria) and cultured in Iscove's Modified Dulbecco's Medium (IMDM) supplemented with 10% fetal bovine serum (Invitrogen, Carlsbad, CA), 50 units/ml penicillin and 50 μg/ml streptomycin (Invitrogen). Cells were cultured at 37 °C in a humidified atmosphere with 5% CO_2 and passaged every 3–4 days. For the MetAP1/2 inhibition experiments, 0.1 μM f.c. Bengamide B (sc-397521A, Santa Cruz Biotechnology, Dallas, TX) was added to HAP1 cells cultured at about 80% of confluency. For proteome-analyses, cells were harvested after 24 h of treatment.

Immunoblot Analysis—Cold PBS washed HAP1 cells were lysed for 5 min on ice in RIPA buffer (50 mM Tris-HCl pH 8.0, 150 mM NaCl, 1% Nonidet P-40) with protease inhibitors added (Roche, Basel, Switzerland). For MetAP1 detection, HAP1 cells were lysed in urea lysis buffer (9 M urea, 50 mm NH4HCO3 (pH 7.9)) by three rounds of freeze-thaw lysis in liquid in N2. The urea lysates were sonicated (Branson probe sonifier output 4, 50% duty cycle, 3 × 30 s, 1 s pulses) followed by centrifugation for 10 min at 16,100 × *g* (4 °C). All lysates were cleared by centrifugation for 10 min at 16,100 g and protein concentration of the measured using the DC Protein Assay Kit (Bio-Rad, Munich, Germany). Sample loading buffer was added and equal amounts of protein (between 40 μg and 100 μg/sample) were separated by SDS-PAGE (1.0 mm thick 12% polyacrylamide Criterion Bis-Tris XT- gels, Bio-Rad) in MOPS buffer (Bio-Rad) at 150 V. Subsequently, proteins were transferred onto a PVDF membrane. Membranes were blocked for 30 min in a 1:1 Tris-buffered saline and 0.1% Tween-20 (TBS-T) Odyssey Blocking solution (cat n° 927–40003, LI-COR, Lincoln, NE) and probed by Western blotting. Following overnight incubation of primary antibody in TBS-T/Odyssey blocking buffer and three 10 min washes in TBS-T, membranes were incubated with secondary antibody for 1 h in TBS-T/Odyssey blocking buffer followed by 3 washes in TBS-T or TBS (last wash step). The following antibodies were used: rabbit anti-actin (A2066, Sigma, Saint-Louis, MO), mouse monoclonal unprocessed 14-3-3γ (iMet 14-3-3γ) (NB100–407, Novus Biologicals, Littleton, CO), rabbit polyclonal 14-3-3γ (orb128923, Biorbyt, Cambridge, UK), rabbit polyclonal anti-MetAP1 (NBP1–53088, Novus Biologicals), rabbit polyclonal anti-MetAP2 (orb33856, Biorbyt), rabbit anti-COTL (orb39513, Biorbyt), mouse monoclonal anti-cytokeratin 18 (ab668, Abcam, Cambridge, UK), rabbit anti-CRABP2 (orb32974, Biorbyt), rabbit anti-RL26A (ab59652, Abcam), rabbit anti-DUSP9 (orb338892, Biorbyt), rabbit anti-HMGCS (orb36825, Biorbyt), anti-mouse (IRDye 800 CW goat anti-mouse antibody IgG, LI-COR, cat n° 926–32210) and anti-rabbit (IRDye 800CW goat anti-rabbit IgG, LI-COR, cat n° 926–32211). The bands were visualized using an Odyssey infrared imaging system (LI-COR) and the intensity of bands assessed using the LICOR Odyssey software for Western blot image processing.

Proteome Sample Preparation for Shotgun Analyses—Cell pellets of WT (HAP1 WT) and METAP1 KO (HAP1 MetAP1 KO) cells obtained from 3 independent cell cultures and containing approx. 10 × 10^6

cells per pellet, were collected and stored at −80 °C until further processing. HAP1 cell pellets resuspended in 400 μl Gu.HCl lysis buffer (4 M GdmCl, 50 mm NH4HCO3 (pH 7.9)) were lysed by three rounds of freeze-thaw lysis in liquid N_2. The lysates were sonicated (Branson probe sonifier output 4, 50% duty cycle, 3 × 30 s, 1 s pulses) followed by centrifugation for 10 min at 16,100 × *g* (4 °C), the supernatant removed and protein concentration determined by Bradford measurement according to the manufacturer's instructions. An aliquot equivalent of 200 μg (~5 × 10^6 cells) was transferred to a clean tube, diluted to 1 mg/ml with lysis buffer, 2× diluted with HPLC grade water, and precipitated with 4× volumes of −20 °C acetone overnight. The precipitated protein material was recovered by centrifugation for 15 min at 3500 × *g* (4 °C), pellets washed twice with −20 °C 80% acetone, and air dried upside down for ~10 min at RT or until no residual acetone odor remained. Pellets were resuspended in 200 μl TFE (2,2,2-trifluoroethanol) digestion buffer (10% TFE, 100 mM ammonium bicarbonate) with sonication until a homogenous suspension was reached. All samples were digested overnight at 37 °C using mass spec grade trypsin/Lys-C Mix (Promega, Madison, WI) (enzyme/substrate of 1:50 w/w) while mixing (550 rpm). Samples were acidified with TFA to a final concentration of 0.5%. Samples were cleared from insoluble particulates by centrifugation for 10 min at 16,100 × *g* (4 °C) and the supernatant transferred to clean tubes. Methionine oxidation was performed by the addition of H_2O_2 to reach a f.c. of 0.5% for 30′ at 30 °C. Solid phase extraction of peptides was performed using C18 reversed phase sorbent containing 100 μl pipette tips (Bond Elut OMIX 100 μl C18 tips (Agilent, Santa Clara, CA) according to the manufacturer's instructions. The pipette tip was conditioned by aspirating the maximum pipette tip volume of water:acetonitrile, 50:50 (v/v) and the solvent discarded. After equilibration of the tip by washing 3 times with the maximum pipette tip volume in 0.1% TFA in water, 100 μl of the acidified samples (~200 μg) were dispensed and aspirated for 10 cycles for maximum binding efficiency. The tip was washed 3 times with the maximum pipette tip volume of 0.1% TFA in water:acetonitrile, 98:2 (v/v) and the bound peptides eluted in LC-MS/MS vials with the maximum pipette tip volume of 0.1% TFA in water:acetonitrile, 30:70 (v/v). The samples were vacuum-dried in a SpeedVac concentrator and re-dissolved in 20 μl of 2 mM tris(2-carboxyethyl)phosphine in 2% acetonitrile.

Proteome Sample Preparation for N-terminal Peptide Enrichment Analyses—Pellets of WT (HAP1 WT) and METAP1 KO (HAP1 MetAP1 KO) cells obtained from 3 independent cell cultures (*i.e.* corresponding cultures of the shotgun proteome analysis) and containing approx. 50 × 10^6 cells per pellet, were collected and stored at −80 °C until further processing. HAP1 cell pellets resuspended in 50 mm NH4HCO3 (pH 7.9) with protease inhibitors added (Roche) were lysed by three rounds of freeze-thaw lysis in liquid N_2 and the lysates cleared by centrifugation for 10 min at 16,000 × *g*. Solid guanidinum hydrochloride was added to the supernatant to a final concentration of 4 M and the protein samples (equivalent of 2 mg) were reduced and S-alkylated. All primary protein amines were blocked using an *N*-hydroxysuccinimide ester of (stable isotopic encoded) acetate at the protein level (*i.e.* an NHS ester of $^{13}C_2D_3$ acetate) to enable the assignment and the calculation of the degree of *in vivo* Nt-acetylation events (25). All modified proteome samples were digested overnight at 37 °C using mass spec grade trypsin/Lys-C Mix (enzyme/substrate of 1:50 w/w) while mixing (550 rpm) and the resulting peptide mixtures vacuum dried. N-terminal peptide enrichment by SCX was performed as described previously (26). The eluted fraction enriched for Nt-peptides were vacuum dried and re-dissolved in 1 ml of 0.5% TFA in 2% acetonitrile. Samples were cleared from insoluble particulates by centrifugation for 10′ at 16,100 *g* and 4 °C, and the supernatant transferred to clean tubes. Methionine oxidation was performed on 100 μl of acidified sample (~200 μg) by the addition of H_2O_2 to reach a f.c. of 0.5% for 30′ at 30 °C. Solid phase extraction of peptides was performed using C18 reversed phase sorbent containing 100 μl pipette tips as described above.

RNA Isolation, RNA Sequencing Library Preparation, Sequencing and mRNA-seq Data Processing—RNA was isolated from HAP1 cells using the TRIzol reagent (Invitrogen) according to manufacturer's instructions. RNA yields were determined using a NanoDrop spectrophotometer (Wilmington, Delaware) and RNA quality was assessed by Agilent Bioanalyzer RNA 6000 Nano Kit. Only samples with RIN values above 9 were accepted. Library generation including random fragmentation, cDNA synthesis and sequencing was performed at the VIB Nucleomics Core (www.nucleomics.be) using the TruSeq stranded total RNA sample preparation kit (Illumina, San Diego, CA) and including a Ribo-Zero (Illumina) depletion step as to remove ribosomal RNA from total RNA by the use of biotinylated Ribo-Zero oligos. Libraries were subjected to sequencing on a NextSeq 500 instrument (Illumina) to yield 75 bp single-end reads, resulting in ~23–28 million 75 bp single end reads per sample. The 3′ adapter sequence (AGATCGGAAGAGCACAC) was trimmed using the fastx_clipper. Reads were pre-mapped onto small nuclear RNA, tRNA and rRNA. The remaining unmapped reads were then mapped onto the human GRCh37 reference genome (Ensembl annotation bundle 75) using STAR 2.4.0i allowing only unique mapping with a maximum of two mismatches. Separate BedGraph files were generated for the sense and antisense strand. Reads were counted across annotated genes using HTseq set to mode "union," feature type "exon" and minimum alignment quality of 10. For the MetAP1 KO cell line, two biological replicate samples were sequenced and for the WT cell line three. The unfiltered reads per kilobase of exon per million fragments (RPKM) values of protein-coding genes displayed a bimodal distribution, where approximately one third of genes had poor mRNA expression (*i.e.* genes with at least one read mapped but with RPKM values below 1), in line with previous reports, (27). Moreover, typically less than 2% of these poorly expressed genes have a corresponding protein expression detected using label-free shotgun proteomics. Therefore, and besides considering only unique reads from the mapping, only protein-coding genes with ≥ 1 RPKM in all biological replicates of both conditions were retained for differential expression analysis. Differential expression analysis was performed using the Bioconductor package DESeq2 (Stanford, CA) in the R statistical programming environment. To determine significantly regulated genes, an adjusted *p* value threshold of 0.01 was applied. The fold change calculations for differentially expressed genes was determined by DESeq2 and represent the log2 change in expression level (*i.e.* counts) for the MetAP1 KO *versus* the HAP1 control setup. RNA-seq sequencing data is accessible through GEO Series accession number GSE103405 in NCBI's Gene Expression Omnibus (28) with reviewer password: *wpuxikegfnkjjkx*.

LC-MS/MS Analysis and Peptide Identification—Peptides were separated by nano-LC and directly analyzed with a Q Exactive instrument (Thermo Scientific, Bremen, Germany) operating in MS/MS mode as described before (29). More specifically, all samples were analyzed via LC-MS/MS on an Ultimate 3000 RSLC nano LC (Thermo Fisher Scientific) in-line connected to a Q Exactive mass spectrometer (Thermo Fisher Scientific). The sample mixture was first loaded on a trapping column (made in-house, 100 μm i.d. × 20 mm, 5 μm beads C18 Reprosil-HD, Dr. Maisch, Ammerbuch-Entringen, Germany). After flushing from the trapping column, the sample was loaded on an analytical column (made in-house, 75 μm i.d. × 150 mm, 3 μm beads C18 Reprosil-HD, Dr. Maisch). Peptides were loaded with loading solvent (0.1% TFA in water) and separated with a linear gradient from 98% solvent A′ (0.1% formic acid in water) to 55% solvent B′ (0.1% formic acid in water/acetonitrile, 20:80 (v/v)) in 30 min at a flow rate of 300 nL/min. This was followed by a 5 min wash

reaching 99% solvent B′. The mass spectrometer was operated in data-dependent, positive ionization mode, automatically switching between MS and MS/MS acquisition for the 10 most abundant peaks in each MS spectrum. The source voltage was 3.4 kV, and the capillary temperature was 275 °C. One MS1 scan (*m/z* 400–2000, AGC target 3×10^6 ions, maximum ion injection time 80 ms) acquired at a resolution of 70 000 (at 200 *m/z*) was followed by up to 10 tandem MS scans (resolution 17 500 at 200 *m/z*) of the most intense ions fulfilling predefined selection criteria (AGC target, 5×10^4 ions; maximum ion injection time, 60 ms; isolation window, 2 Da; fixed first mass, 140 *m/z*; spectrum data type, centroid; underfill ratio, 2%; intensity threshold, 1.7×10^4; exclusion of unassigned, 1, 5–8, >8 charged precursors; peptide match preferred; exclude isotopes, on; dynamic exclusion time, 20 s). The HCD collision energy was set to 25% normalized collision energy, and the polydimethylcyclosiloxane background ion at 445.120025 Da was used for internal calibration (lock mass).

Raw data files were searched with MaxQuant (30) using the Andromeda search engine (31) (version 1.5.4.1) and MS/MS spectra searched against the Swiss-Prot database (taxonomy *Homo sapiens*; 20,195 entries; May 2016 version) for N-terminal proteome analyses, or a two amino acids N-terminally truncated version of the Swiss-Prot database was used to avoid contribution of N-terminal peptide abundances to the overall LFQ protein calculations in case of shotgun proteome analyses. In both cases potential contaminants present in the contaminants.fasta file that comes with MaxQuant were automatically added.

A precursor mass tolerance was set to 20 ppm for the first search (used for nonlinear mass recalibration) and set to 4.5 ppm for the main search. For shotgun proteome analyses, trypsin/P (*i.e.* cleavages among lysine/arginine-proline residues were allowed) was selected as enzyme setting and up to two missed cleavage were allowed. Methionine oxidation was searched as fixed modifications, whereas N-terminal protein acetylation was set as variable modification. In case of N-terminal proteome enriched samples, ArgC was selected as enzyme setting as cleavage after lysine residues is obstructed by acylation of their side chains. Cleavages among arginine-proline residues were considered and semi-specific free N terminus was chosen as digestion mode. Methionine oxidation, carbamidomethylation of cysteines and heavy acetylation at lysine side-chains (Acetyl:2H(3)C13(2) (K)) were searched as fixed modifications, whereas acetylation and heavy (Acetyl:2H(3)C13(2) (N-term)) acetylation on protein N termini were set as variable modifications. The false discovery rate for peptide and protein identification was set to 1%, and the minimum peptide length was set to 7. The minimum score threshold for both modified and unmodified peptides was set to 40. The match between runs function was enabled and proteins were quantified by the MaxLFQ algorithm integrated in the MaxQuant software (32) in case of shotgun proteome analysis. Here, a minimum of two ratio counts and only unique peptides were considered for protein quantification.

The mass spectrometry proteomics data (*i.e.* the total list of identified proteins and modified peptides (next to the evidence file) in case of shotgun and N-terminal proteomics respectively)) have been deposited to the ProteomeXchange Consortium via the PRIDE (33) partner repository with the data set identifier PXD006638. Annotated, mass-labeled MS/MS spectra can be viewed on MS-Viewer (http://msviewer.ucsf.edu/prospector/cgi-bin/msform.cgi?form = msviewer) (34) using the search keys umhkpodlaj (supplemental Table S2*A*), 4adxtut9up (supplemental Table *S2B*) and 7balnvbgbr (for the 33 peptides corresponding to single-peptide based protein identifications in supplemental Table S3). In case of the supplemental Table S2*B* data set, only assigned ion peaks are visualized on MS-Viewer. Complete annotated spectra can be viewed using the deposited data and MaxQuant Viewer.

Quantification of the Degree of Protein Nt-acetylation—To quantify the degree of protein *in vivo* Nt-acetylation, raw data files were searched with Mascot using the Mascot Daemon interface (version 2.5.1, Matrix Science) and MS/MS spectra searched against the Swiss-Prot database (taxonomy *Homo sapiens*; 20,172 entries; January 2017 version). The Mascot search parameters were set as follows; methionine oxidation to methionine-sulfoxide, heavy acetylation at lysine side-chains (Acetyl:2H(3)C13(2) (K)) and carbamidomethylation of cysteine were set as fixed modifications. To enable identification quantification of the degree of Nt-acetylation, acetylation *versus* heavy acetylation of N termini (Acetyl:2H(3)C13(2) N-term) was selected as quantification option, and carried out using the Mascot Distiller Quantitation Tool (version 2.5.1.0). Mass tolerance was set to 10 ppm on the precursor ion (with Mascot's C13 option set to 1) and to 20 mmu on fragment ions. Peptide charge was set to 1+, 2+, 3+ and instrument setting was put to ESI-QUAD. Endoproteinase semi-Arg-C/P (Arg-C specificity with arginine-proline cleavage allowed) was selected as enzyme allowing for 1 missed cleavage.

In case of N-terminal peptide analyses, only peptides that were ranked one, have a minimum amino acid length of seven, scored above the threshold score set at 99% confidence, displayed a start position of 1 or 2 and belonged to the category of N termini compliant with the rules of initiator methionine (iMet) processing (10) or represented actin N termini, were withheld. More specifically, iMet processing was considered in the case of iMet-starting N termini followed by any of the following amino acids; Ala, Cys, Gly, Pro, Ser, Thr, Met, or Val. Data management was done in ms_lims (35). Whenever the degree of protein *in vivo* Nt-acetylation could be calculated for Mascot identifications with Mascot Distiller based quantifications, data was considered for the analysis reported under the section 'Proteome-wide characterization of Nt-acetylation profiles' in case of matching MaxQuant N-terminal peptide identifications.

Software Packages for Statistics and Data Visualization—For basic data handling, normalization, statistics (if not stated otherwise), and annotation enrichment analysis, we used the freely available open-source bioinformatics platform Perseus (version 1.5.3.2) (36). Perseus was used for nonsupervised hierarchical clustering and the generation of heat maps, profile and scatter plots. Furthermore, 1D and 2D annotation enrichment analysis was performed using the Perseus software (37) with a two-sided test with Benjamini-Hochberg FDR correction. Data analysis after uploading the protein groups file obtained from MaxQuant database searching was performed as described previously (38). All replicate samples were grouped and LFQ-intensities log(2) transformed. Proteins with less than three valid values in at least one group were removed and missing values were imputed from a normal distribution around the detection limit (with 0.3 spread and 1.8 downshift).

Experimental Design and Statistical Rationale of the Proteome and Transcriptome Analyses—We analyzed the proteomes and matching N-terminal proteomes of a subset of 12 samples corresponding to 3 biological triplicates per setup *i.e.* WT, MetAP1 KO, and Bengamide B treated WT and MetAP1 KO HAP1 cells) using a label-free intensity based proteomics approach. In addition, we profiled matching transcriptomes of non-inhibitor treated samples corresponding to at least two biological replicates per condition. More specifically, for the MetAP1 KO cell line, two biological replicate samples were sequenced and for the WT cell line three biological replicate samples.

Lens-free Cell Imaging and Calculation of Cell Doubling—Holographic lensless imaging of cell cultures grown in parallel was performed using Cytonote devices from Iprasense with a resolution of 1–2 μm. By placing the Cytonote devices consisting of a LED for illumination and a CMOS image sensor in contact with the cell culture vessels (*i.e.* 25 cm^2 falcons) in an incubator, the interference pattern with the sample (*i.e.* the interference between the partially coherent

incident light and the light scattered by the cells in culture) was captured. From the holographic pattern, the sample image is reconstructed by applying the Horus software, including cell segmentation and basic analysis functions. The extremely wide field of view (30 mm^2) results in relevant statistics from single images.

Confluency of cell culture monitored using lens-free imaging over the course of 24 h before the addition of Bengamide B and the following 48 h, was fitted with an exponential model using the Doubling Time Online Calculator (http://www.doubling-time.com/compute.php). Cell doubling time was calculated from the assigned growth rate as follows: ln(2)/growth rate and represented in hours.

RESULTS

To elucidate the omics-wide effects of MetAP perturbation and to study the redundant action and proteome-wide substrate specificity profiles of human MetAP1 and MetAP2 in general, an attempt was made to create human MetAP1 and MetAP2 knockout cells in the HAP1 haploid cell line. Using CRISPR/Cas9 editing, the Cas9 endonuclease is targeted by a pair of guide RNAs to generate double stranded DNA breaks, a process followed by non-homologous end-joining (NHEJ) repair that is accompanied by a precise DNA deletion of the locus of interest (39). By producing frameshift mutants of the gene of interest, CRISPR/Cas9 editing can generate custom human knockout cells. Consequently, genome engineering using CRISPR-mediated gene knockout is especially straightforward in haploid human cell lines and this way, frameshift mutants were obtained for MetAP1 and MetAP2 in HAP1 cells. However, as confirmed by Western blotting analysis and the mass spectrometric detection of MetAP1 (identified based on the exclusive detection of 6 unique peptides in merely all (inhibitor-treated) WT setups) (Fig. 1*A*), a functional mutant clone (*i.e.* a 179 bp insertion in exon 4 (see Experimental Procedures)) was obtained only in case of MetAP1. In case of MetAP2, the frameshift resulted in the production of an N-terminally truncated MetAP2 proteoform which still retained (part of) its activity as deduced from the unaltered iMet retention profiles observed (data not shown). Interestingly, despite the unaltered MetAP2 expression observed at the transcript level (supplemental Table S1), a 2- and 4-fold increase of MetAP2 was observed at the proteome level in case of Bengamide B treated wild type cells or in MetAP1 KO cells and Bengamide B treated MetAP1 KO cells, respectively (Fig. 1*A*).

MetAP1 Knockout Cells Display Altered Proliferation Rates and Cellular Morphology Next to Increased Sensitivity Toward MetAP Inhibition—Because MetAP1 and/or MetAP2 inhibition was previously linked to altered cell proliferation, we first determined the effects of MetAP1 knockout and chemical MetAP inhibition—using Bengamide B as a nanomolar inhibitor of MetAPs 1 and 2 (24)—on cell proliferation. Using time lapse data obtained by lensless cell culture imaging of cells in culture; cell densities, cell sizes and growth rates of WT and MetAP1 mutant cells were quantitatively evaluated and compared. As deduced from the monitored confluency measurements of cell cultures before and after the addition of Bengamide B (Fig. 1*B*), cell doubling time calculations revealed a near 2-fold increase in the doubling time of MetAP1 knockout *versus* WT cells (*i.e.* from 17 h to 31 h) when monitoring confluency during the first 24h after platting. Interestingly, although the proliferation rates of WT HAP1 remained essentially unaltered during the next 24 h of cultivation, the doubling rate of MetAP1 knockout cells more closely approached that of WT cells (*i.e.* 20 h), indicating a delay in cell proliferation, especially during the first phase after plating. The difference in cell doubling becomes even more pronounced on addition of the MetAP inhibitor Bengamide B. Here a doubling time of 28 h was observed in the case of Bengamide B treated WT cells, whereas 75 h was required to achieve cell doubling of Bengamide B treated MetAP1 knockout HAP1 cells (*i.e.* an over 4-fold increase in doubling time as compared with its isogenic WT counterpart). As such, a correlation between the loss of MetAP1 expression and its inhibitory effect on cell proliferation can clearly be observed (Fig. 1*B*), indicating that the lack of MetAP1 expression in HAP1 cells can not entirely be compensated for by the increased MetAP2 expression levels observed (Fig. 1*A*). Interestingly, although a fibroblast-like morphology can be observed in case of both HAP1 cell lines, MetAP1 mutant cells show on average a 30% increase in attached cell size (*i.e.* from 17 to 22 μm in diameter) (Fig. 2). Because MetAP1 has previously been implicated in cell cycle progression through G_2/M phase (40), a delayed G_2/M phase progression can likely account for this observation.

Impaired iMet Processing of the Known MetAP1/2 Substrate 14-3-3γ in MetAP1 Knockout Cells—Next, we assessed the functional effect of the introduced frameshift mutation in MetAP1 by probing the extent of iMet retention of the known MetAP1/2 substrate, 14-3-3γ (24) (*i.e.* iMet-14-3-3γ), a protein previously shown to act as a cellular indicator for the combined readout of (perturbed) MetAP activity in human (41).

As a reference sample, Bengamide B treated cells were sampled in parallel. Here, the inhibitor was used at a final concentration of 0.1 μg per ml for 24h of incubation. Using a monoclonal antibody raised against an N-terminal peptide corresponding to the iMet unprocessed N terminus of 14-3-3γ (*i.e.* iMet-14-3-3γ), changes in MetAP dependent iMet processing efficiencies of iMet-14-3-3 γ could be monitored.

When compared with total 14-3-3 γ protein levels, the basal levels of iMet-14-3-3γ increased about 50% in untreated MetAP1 KO cells (Fig. 3) whereas on Bengamide B treatment, a 3.4 fold and 4 fold increase of iMet-14-3-3γ was observed in case of WT cells and MetAP1 KO cells, respectively. As such, MetAP1 deletion clearly reduces the efficiency of iMet-14-3-3γ processing and the use of higher concentrations or prolonged incubation with Bengamide B didn't lead to a further increase of iMet-14-3-3γ (data not shown). Noteworthy, a cell dependence in the increase in the ratio of unprocessed *versus* total 14-3-3γ on Bengamide B treatment has been

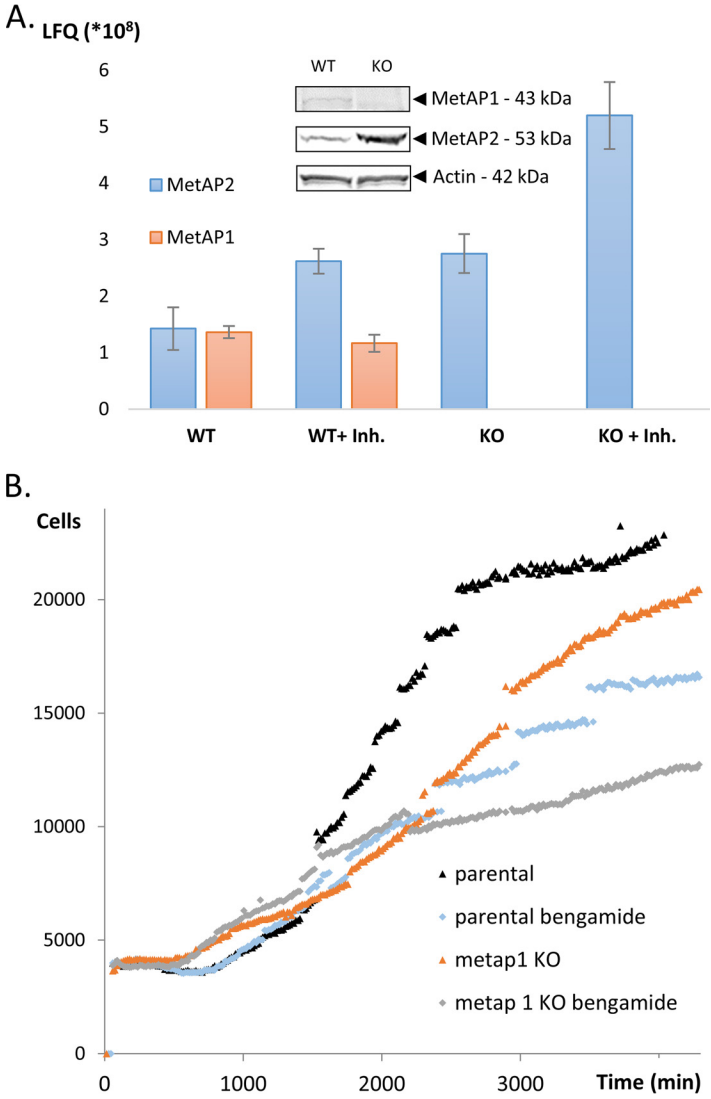

FIG. 1. ***A*, MetAP protein expression analysis in MetAP1 KO HAP1 cells and on MetAP inhibition.** LFQ values of MetAP1 (orange) and MetAP2 (blue) are shown for all four setups analyzed. Bars represent the average values of three biological repeats and the error bars represent standard deviations of these values. Protein quantification values of MetAP1 and MetAP2 were based on the identification of 6 and 13 unique peptides, respectively. In the inset, Western blotting analyses of corresponding HAP1 WT and MetAP1 KO cell lysates are shown immunoblotted with antibodies specific for MetAP1, MetAP2 and β-actin. *B*, Deletion of MetAP1 in HAP1 cells reduces cell proliferation rates in analogy to chemical MetAP inhibition. Cell proliferation of WT and MetAP1 mutant HAP1 cells monitored by lens-free imaging over a period of 72 h. Acquisition and phase reconstruction of cultures of human WT and MetAP1 mutant HAP1 cells seeded at 2–5% confluency, incubated at 37 °C and treated with vehicle or Bengamide B after 24h of cultivation was performed. Cell counts were recorded in a 29.4 mm^2 field of view containing about 20,000 cells on confluency in case of HAP1 WT cells. The results shown are representative for two independent experiments.

reported previously, further hinting to cell type dependent MetAP efficiencies.

Proteome-wide Characterization of iMet Retention Profiles—N-terminal proteome enriched replicate samples were analyzed by 1D nano LC-MS/MS using 3h gradients on a quadrupole Q Exactive Orbitrap instrument (42) and subjected to label-free, ion intensity-based peptide quantitation and quantification of the degree of N-terminal acetylation (see below) using MaxQuant (30) and Mascot respectively. N-terminal peptide enrichment was used to investigate proteome-wide alterations in iMet retention on genetic MetAP1 deletion and/or chemical MetAP inhibition among others. More specifically, 3 biological replicate proteome samples were obtained in case of WT, MetAP1 KO and Bengamide B treated WT and MetAP1 KO HAP1 cells.

In case of N-terminal proteome enriched samples, all samples were reduced and *S*-alkylated and the primary protein amines blocked using an *N*-hydroxysuccinimide ester of (stable isotopic encoded) acetate at the protein level (*i.e.* an NHS ester of $^{13}C_2D_3$-acetate) to enable the assignment and the calculation of the degree of *in vivo* Nt-acetylation (see below) (43). N-terminal peptide enrichment by SCX was performed as

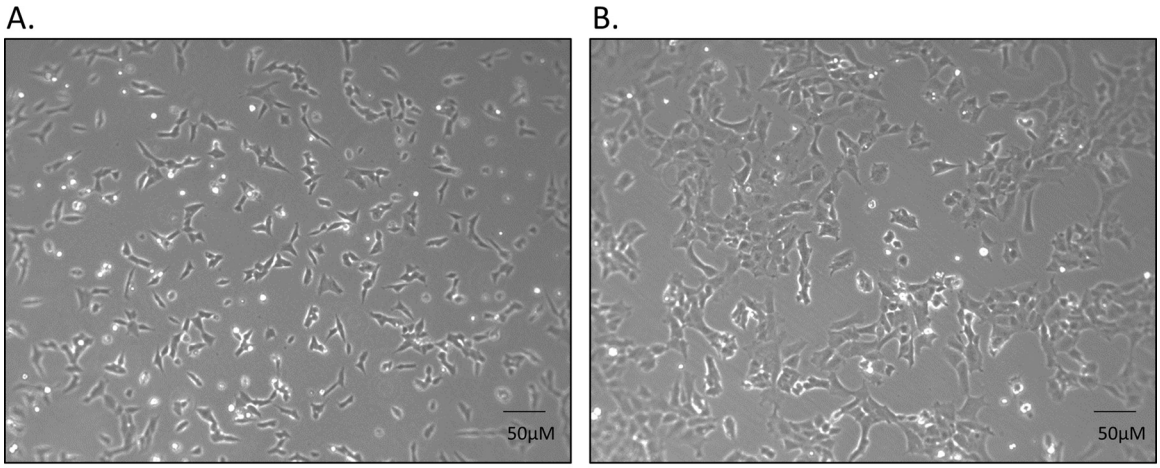

FIG. 2. **Altered size and morphology of MetAP1 KO HAP1 cells.** Acquisition and phase reconstruction of cultures of human WT and MetAP1 mutant HAP1 cells. Mean cell diameter of WT (*A*) and MetAP1 (*B*) mutant cell cultures are indicated in μm. The difference in size between WT and MetAP1 KO HAP1 cells was statistically significant ($p < 0.001$, student *t* test).

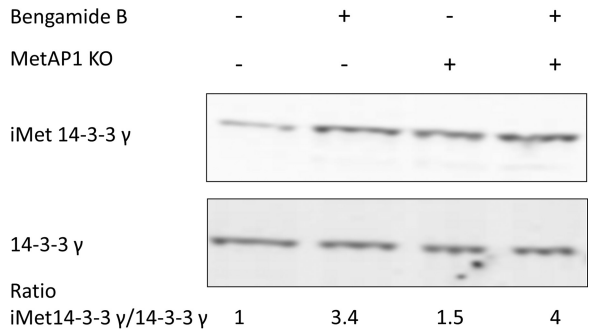

FIG. 3. **Impaired iMet processing of 14-3-3γ in MetAP1 knockout HAP1 cells.** HAP1 MetAP1 KO or WT cells were treated with vehicle (DMSO) or Bengamide B for 24 h. Cell lysates were resolved by SDS-PAGE, transferred to PVDF membrane, and immunoblotted with antibodies specific for 14-3-3γ or iMet 14-3-3γ (*i.e.* the iMet unprocessed form of 14-3-3γ). The levels of iMet 14-3-3γ were quantified by densitometry and then normalized to 14-3-3γ.

described previously (2). The eluted fractions enriched for N-terminal peptides were subjected to 1D LC-MS/MS analysis. When using the Andromeda and Mascot peptide search engines, 1767 iMet compliant (see methods) protein N termini derived from 1282 human proteins were identified in total (supplemental Tables S2*A* and S2*B*). Of these N termini, 1506 started at position 1 or 2, whereas 261 had a start position beyond protein position 2. As reported previously, the latter category of N termini are indicative of alternative translation initiation events (44, 45). Of the 1631 N termini with intensity-based peptide MaxQuant quantification data (supplemental Table S2*A*), 407 N termini were identified in all setups analyzed (25% of all identified protein N termini).

When performing a 1D annotation enrichment (37) on the modified N-terminal peptide intensities obtained using MaxQuant (supplemental Table S2*B*), and only considering iMet compliant categories of N termini (*i.e.* A, MA, C, MC, MD, ME, MF, G, MG etc.), significant changes ($p < 0.01$) in the abundance of certain N-terminal categories in the MetAP1 KO could be observed when compared with the WT setup (Fig. 4).

More specifically, the steady state levels of MS-, MP-, and MA- N termini are significantly increased in the knockout as compared with their WT levels, whereas their processed counterparts (*i.e.* S- and A- N termini) are significantly reduced. MV-, MT-, and MG- termini are only significantly affected on MetAP inhibition in general or by the additional inhibition of MetAP2 in MetAP1 knockout cells (Fig. 4*A*). Peptide intensity profile plots also reflect these significant changes observed (Fig. 4*B*).

Proteome-wide Characterization of Nt-acetylation Profiles—Because our previous work revealed a kinetic competition between NATs and MetAPs (20), we also assessed (potential differences in) protein Nt-acetylation levels.

Overall, as deduced from the very high correlation observed, the degree of Nt-acetylation remained essentially unaltered when comparing the Nt-acetylomes of the different setups analyzed (supplemental Fig. S1 and supplemental Table S2*A*). This observation hints to the fact that the degree of iMet processing has only minor effects on the steady-state Nt-acetylation levels of Nt-proteoforms whenever detectable (*i.e.* iMet-processed and iMet unprocessed Nt-proteoforms).

Interestingly however, 3 MAP-starting N termini displayed on average a 25% increase in the degree of Nt-acetylation observed when comparing the MetAP1 KO to the WT setup (*i.e.* MTHFD1, EIF2A and ATIC) (supplemental Fig. S1), whereas several (iMet unprocessed) NatA type substrate N termini were also substantially affected in their degree of Nt-acetylation when comparing inhibitor treated MetAP1 KO *versus* inhibitor treated WT setups.

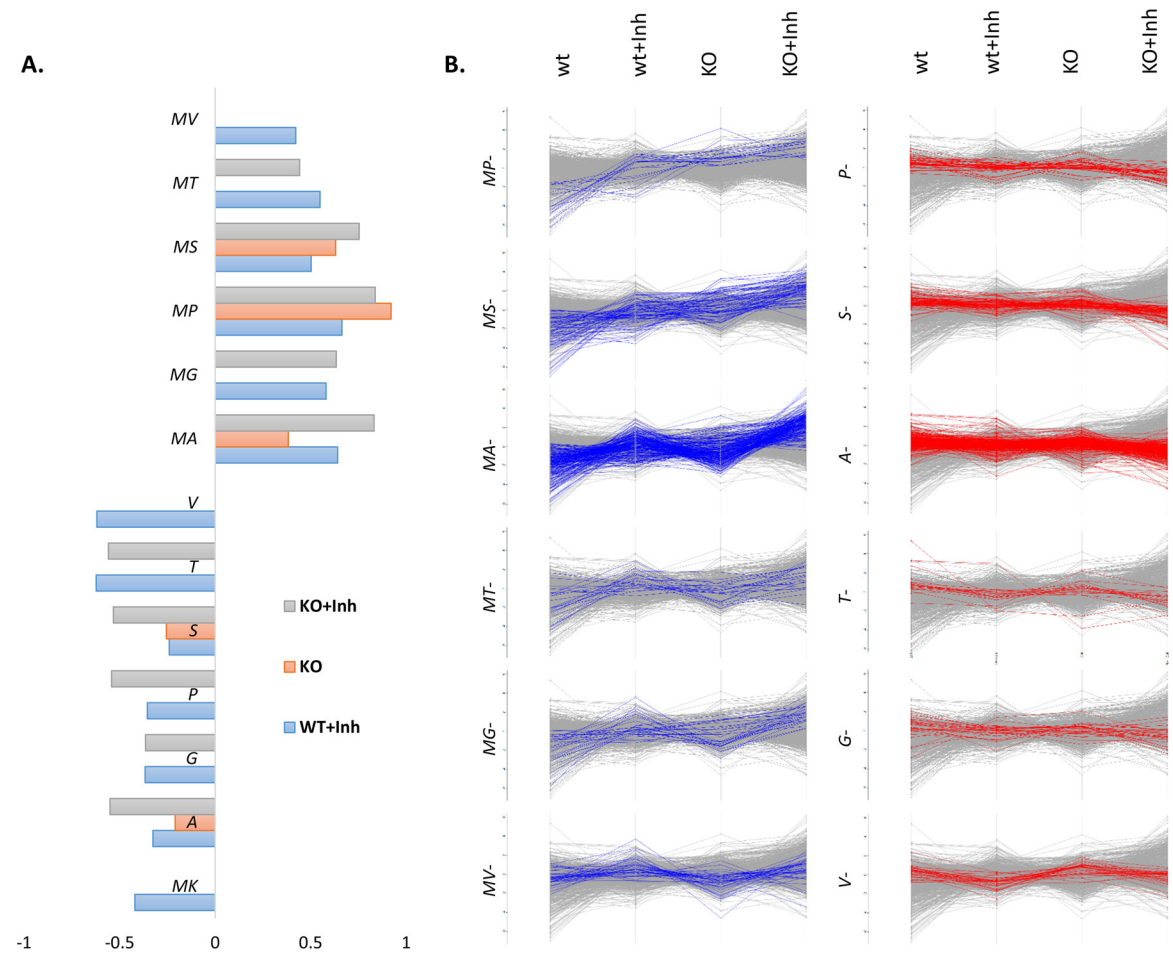

FIG. 4. **Proteome-wide characterization of iMet retention profiles.** *A*, Bar chart representation of significantly regulated (FDR < 1%) normalized enrichment scores (-1 to +1 max) of N-terminal categories are shown for the KO, KO + Inh. or WT + Inh. *versus* WT setups. (left: down in KO, KO + Inh. and/or WT + Inh.; right: up in KO, KO + Inh. and/or WT + Inh.). Term enrichment was determined using the 1D annotation enrichment algorithm embedded in the Perseus software suite and *p* values were corrected for multiple hypotheses testing using the Benjamini and Hochberg false discovery rate. Only corrected *p* values <0.01 were considered. *B*, Individual profile plots of normalized N-terminal peptide intensities across all four conditions assayed are shown. N-terminal categories for which N termini with significantly altered abundancies could be observed (except for MK- N termini) were highlighted in red and blue in case of iMet-processed and iMet-retaining N termini, respectively.

Shotgun Proteome Analysis Reveal Changes in Protein Expression Profiles on Perturbation of MetAP Activity of Proteins Implicated in Lipid Metabolism, Cytoskeleton Organization, and Protein Synthesis—Shotgun proteome analysis was performed to monitor quantitative differences in steady-state protein expression levels by high-resolution mass spectrometry (MS) based proteomics using single LC runs and label-free protein quantitation (32). Of the 3 biological replicate samples analyzed per setup (*i.e.* WT, MetAP1 KO and Bengamide B treated WT and MetAP1 KO HAP1 cells) and thus 12 proteome samples analyzed in total, 4971 unique proteins could be identified at a peptide and protein false discovery rate (FDR) of 1%. Label-free quantification was performed to enable relative proteome comparisons (see also methods) by use of the intensity values (LFQ) obtained using the MaxLFQ algorithm (30, 32). Of note, N-terminal peptide intensities were not considered for the LFQ calculations to avoid contribution of N-terminal peptide abundances to the overall LFQ protein calculations (see methods). After log2 transformation of the obtained LFQ values, a multiscatter plot was calculated together with the Pearson correlation. The very high Pearson correlations observed (*i.e.* an average Pearson correlation of 0.98 and all above 0.95) between the different replicates and samples analyzed overall point to the high reproducibility of the chromatographic separations and MS detectability among the different runs (supplemental Fig. S2). Protein expression profiling using a two-way ANOVA test was performed to reveal proteins of which the expression level significantly differs between the genotype ($p < 0.001$) and treatment samples ($p < 0.01$). Log2 transformed LFQ values were grouped for all replicate samples and only proteins with minimally 3 valid values in at least one setup were considered, overall permit-

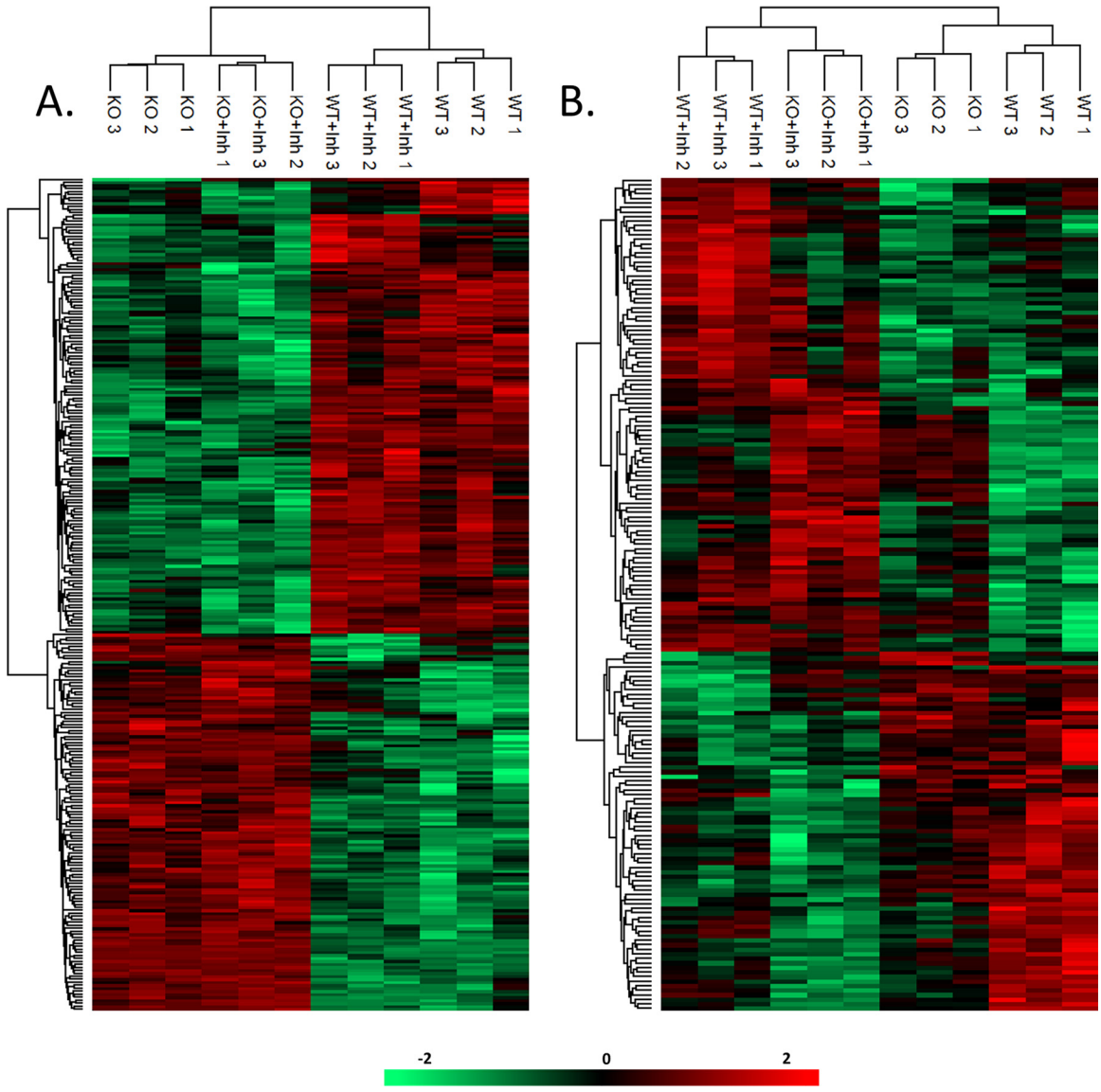

FIG. 5. **Z score heat map representations of cluster analysis reveal proteins with differential abundance dependent on genotype or treatment.** Non-supervised hierarchical clustering of *z*-scored MS intensities of significant genotype (WT or MetAP1 KO) (*A*) and treatment (untreated or Bengamide B treatment) (*B*) regulated proteins after two-way ANOVA are represented. 278 protein groups were found significantly regulated dependent on the genotype ($p < 0.001$) and 183 protein groups dependent on Bengamide B treatment ($p < 0.01$) (supplemental Table S3). Green indicates low intensities whereas red indicates high intensities.

ting differential protein expression analysis of 3,386 unique proteins (supplemental Table S3). Missing data values were replaced with imputed values from the corresponding normal distribution around the detection limit. Overall, 278 protein groups were found significantly regulated dependent on the genotype ($p < 0.001$) and 183 protein groups dependent on Bengamide B treatment ($p < 0.01$). The intensities of significantly regulated proteins are shown as heat maps after z-score transformation and non-supervised hierarchical row clustering (Fig. 5).

Relative enrichment of the indicated gene categories (UniProt keywords) calculated using the 1D annotation enrichment algorithm (37) point to significant expression changes ($p < 0.02$) in four main protein categories linked to the terms; "protein synthesis," "organelle," "lipids/membrane," and "cell connection/cytoskeleton" (Fig. 6). Although all four categories were affected on MetAP1 deletion (*e.g.* downregulation of protein synthesis and lipid metabolism, and upregulation of cytoskeletal proteins), only proteins implicated in protein synthesis and more specifically ribosome biogenesis were found to be significantly downregulated on Bengamide B treatment of control cells.

Western blot analyses were performed to substantiate some of the genotype and/or inhibitor dependent quantitative changes observed in the protein expression levels. When probing for the differentially expressed proteins COTL1,

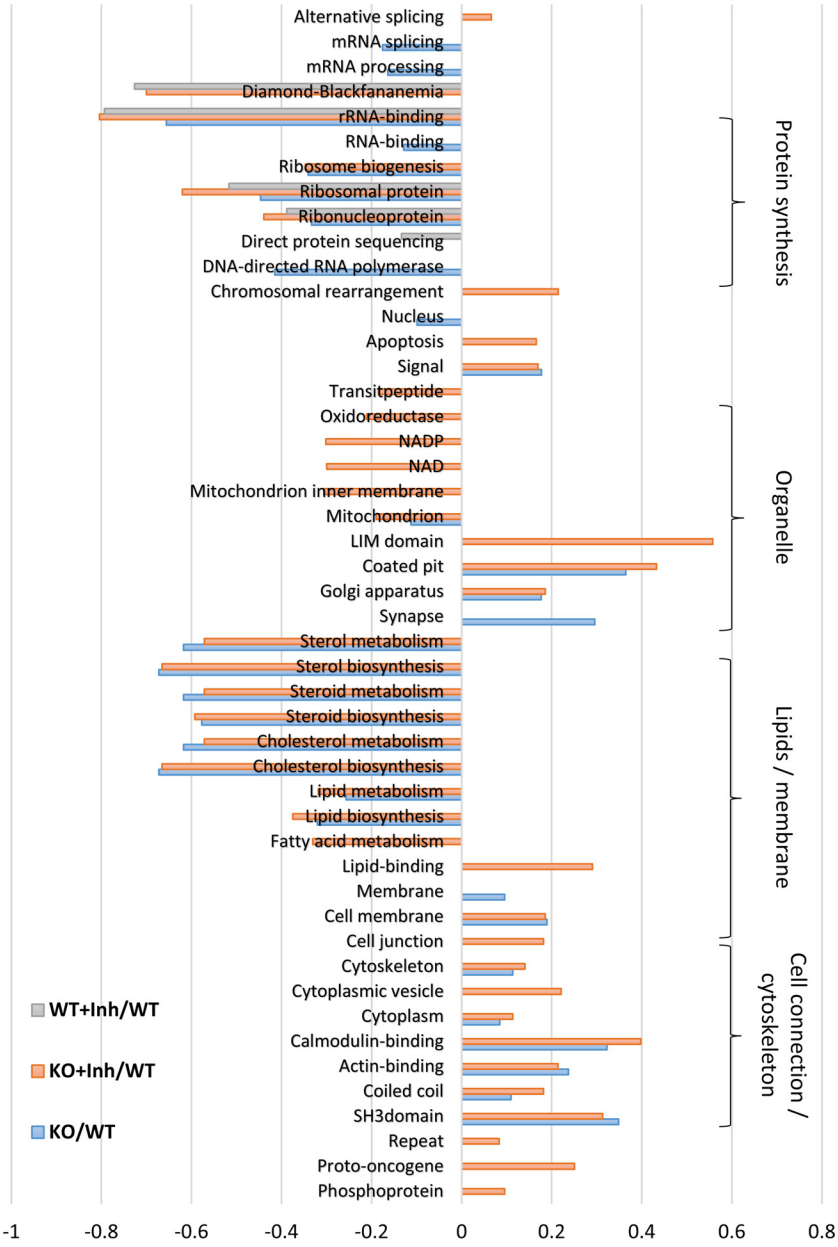

FIG. 6. **Bar Chart representation of normalized annotation enrichment scores.** Bar Chart representation of significantly regulated (FDR < 2%) normalized annotation enrichment scores (−2.5 to +1 max) of UniProt keyword annotations are shown for the KO, KO + Inh. or WT + Inh. *versus* WT setups. (left: down in KO, KO + Inh. and/or WT + Inh.; right: up in KO, KO + Inh. and/or WT + Inh.). Term enrichment was determined using the 1D annotation enrichment algorithm embedded in Perseus (36, 37) and *p* values were corrected for multiple hypotheses testing using the Benjamini and Hochberg false discovery rate. Only corrected *p* values <0.02 were considered.

KRT18, CRABP2, RL26A, DUSP9, and HMGCS (Fig. 7), both methods were found to be in excellent agreement.

Protein Expression Changes in the Context of Protein N-terminal Amino Acid Identity and Transcript Levels Using Deep Transcriptomics—In line with the unaffected steady-state protein levels of the MetAP1/2 substrate 14-3-3γ (Fig. 3 and supplemental Table S3), when performing annotation enrichment of protein N-terminal identities and using the 1D annotation enrichment algorithm (37) on the normalized protein intensities and independent of iMet processing (*i.e.* all 20 possible categories were considered MA, MC, MD, ME, …), no significant difference in the occurrence of N-terminal protein identities could be observed when comparing regulated *versus* nonregulated proteins.

Further, we systematically compared the transcriptome and proteome changes on MetAP1 knockout. When only considering the shotgun proteomes of untreated control and MetAP1 KO cells, for 97% of the proteins quantified by MS, a transcript abundance estimate was obtained by means of RNA sequencing (supplemental Table S1). The Pearson cor-

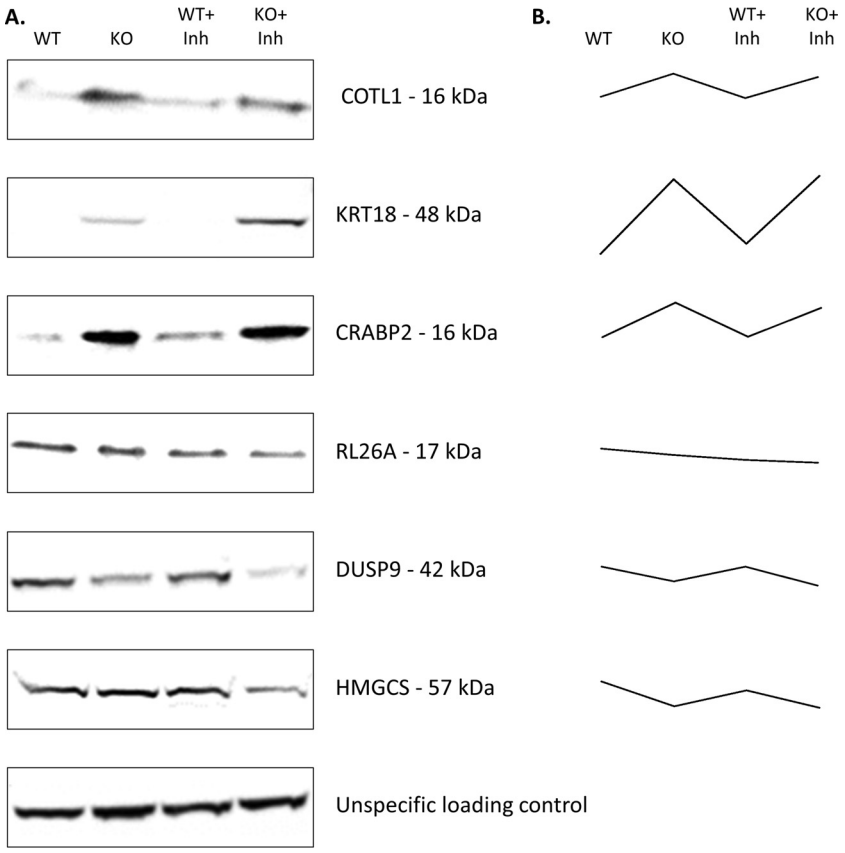

FIG. 7. **Western blot validation of genotype and/or inhibitor dependent quantitative proteome changes observed.** *A*, Western blotting results and *B*, LFQ based expression changes observed are shown in case of COTL1, KRT18, CRABP2, RL26A, DUSP9 and HMGCS. An unspecific loading control is indicated as reference.

relation of transcript and protein abundance was found to be ~0.6 (Figs. 8*A* and 8*B*). The correlation of mRNA abundance ratios with protein abundance ratios was moderate (Pearson $r = 0.28$) (Fig. 8*C*).

By performing a gene ontology term enrichment analysis to charachterize global effects on the transcript as well as proteome level, a 2D annotation enrichment analysis (37) was performed based on a nonparametric Mann-Whitney test (FDR < 0.02) using the Perseus software (36) (Fig. 9). Although the effect on processes linked to cell proliferation was mainly reflected in the reduced transcript levels, processes such as DNA replication and sterol biosynthesis were downregulated both at the transcriptome and proteome level in MetAP1 knockout cells. Consistent with the antiproliferative effect of MetAP1 inhibition and reflected in the lowered abundancy of a multitude of ribosomal proteins (supplemental Table S3), downregulation of (mitochondrial) translation processes was also found to occur at both omics levels.

Processes upregulated at the transcript and steady-state proteome level of MetAP1 knockout cells include the positive regulation of cell adhesion and extracellular structure organization next to secretory processes such as vesicle organization, exocytosis and Golgi vesicle transport. Furthermore, although a(n) (slight) upregulation of proteins implicated in protein folding (*e.g.* chaperonnes) and the biosynthesis of nucleobase-containing compounds could be observed, the corresponding mRNA levels were downregulated.

DISCUSSION

Although chemical inhibition and knockdown studies on the topic of MetAPs have been reported previously, the high efficiency of iMet excision and incompleteness of inhibition or knockdown next to the redundant actions of MetAPs observed precludes general conclusions of independent MetAP activities. Although both MetAPs have been listed as "core essentialome" components in the human haploid HAP1 cell line and thus likely represent highly essential proteins (46), a functional MetAP1 mutant HAP1 clone edited by CRISPR/Cas to contain a frameshift mutation in the fourth coding exon was nonetheless successfully obtained. The use of isogenic human haploid cells in a variety of genetic studies, confirms the validity of the use of the HAP1 haploid cell line (or its parental line KBM7) as a model system compared with a "standard" diploid cell line.

With this cell model at hand, we pursued to study the omics-wide effect of MetAP1 deletion and general MetAP inhibition. In line with previous reports, a correlation between MetAP expression levels and cellular MetAP inhibitory effect could be observed. Further, iMet retention levels were inversely correlated with cellular proliferation rates.

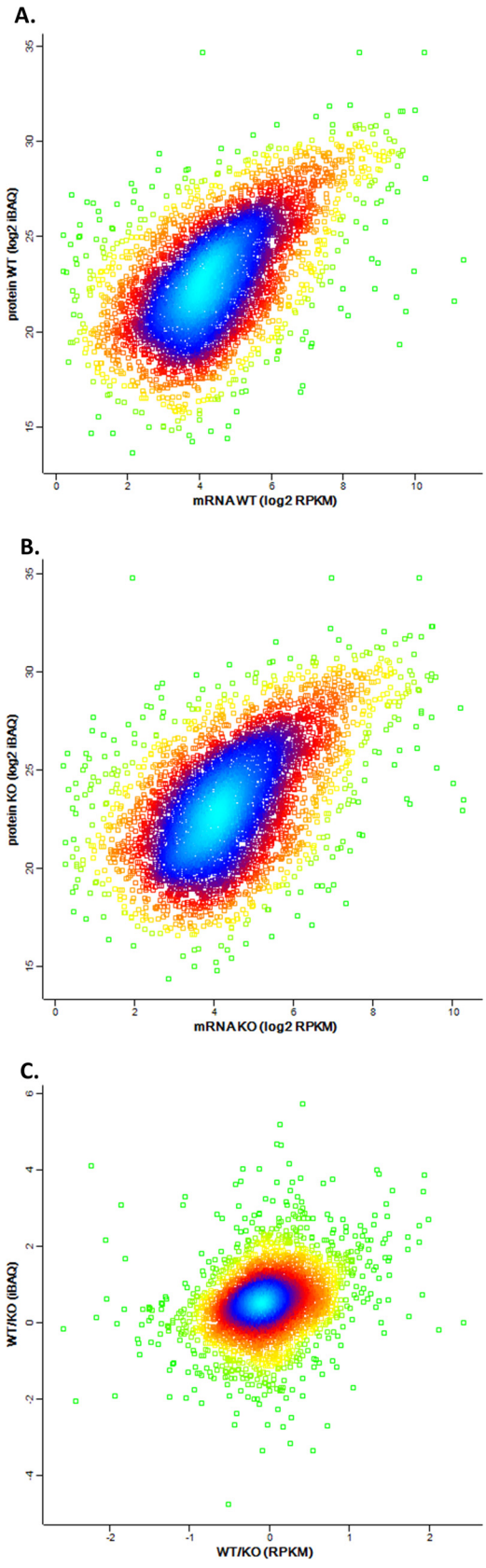

Because ectopic MetAP expression and protein expression levels of MetAPs was reported to be positively correlated with the increased resistance of cell lines against MetAP inhibition (47, 48), the specific increase in MetAP2 expression levels observed on MetAP1 deletion and/or MetAP inhibition, points to reprogramming of the cell enabling the cell to cope with the loss of MetAP.

Further, iMet retention profiles determined by positional proteomics revealed statistically significant changes in the steady-state abundances of (M)S-, (M)P- and MA- N termini. More specifically, iMet-retaining and iMet-processed proteoforms of these N termini were found to be respectively up- and downregulated in the MetAP1 KO cells. On additional inhibition of MetAP2 or MetAP inhibition in general, all NatA type N termini (M)S-, (M)A- and M(P)-, (M)T-, (M)V- and (M)G- were affected, meaning that iMet processing of MV-, MT- and MG- termini were only found significantly affected on (additional) inhibition of MetAP2. This observation might be explained by the (partially) overlapping specificity of MetAP1 and MetAP2 (in line with Frottin *et al.* (10)), which in case of MetAP1 deletion and for MV-, MT- and MG- termini was compensated for by (the increased expression of) MetAP2. More likely however, in line with the previously determined *in vitro* substrate specificity profiles of MetAP1 and MetAP2, MetAP2 may display a much higher or even exclusive action over these type of N termini (11). More specifically, Xiao *et al.* showed that the catalytic activity of human MetAP1 toward MV- and MT- peptides was up to two orders of magnitude lower than that of MetAP2 pointing to the fact that MetAP2 is mainly responsible for processing of MV- and MT- N termini (11).

Nonetheless, MetAP2 is unable to restore levels of iMet processing observed in case of MS-, MP-, and MA- N termini, indicating the manifold higher or exclusive activity of MetAP1 over these type of N termini.

Viewing the previously revealed kinetic competition between NATs and MetAPs (20), to our surprise, only few protein N termini (*e.g.* MAP- starting N termini) were identified as differentially Nt-acetylated when comparing the Nt-acetylomes of WT and MetAP1 KO cells. The effect observed is likely because of Nt-acetylation being unable to keep up with the increased levels of specific iMet-retaining N termini of nascent polypeptides, making them more easily observable in case of sub-optimal NAT substrates, including MAP- N termini displaying a proline at position 3, a residue known to

Fig. 8. **Density-enhanced scatterplots between proteome and transcriptome expression levels comparing WT and MetAP1 knockout HAP1 cells.** Per gene and only in case of two valid replicate values for the proteome and transcriptome setups analyzed, mean RPKM values were compared with their corresponding mean iBAQ (intensity based absolute quantification) values (51). Pearson correlations values of 0.584 (*A*) and 0.549 (*B*) were observed in case of WT and KO proteome samples, respectively. *C*, When comparing mRNA with protein abundance ratios, the Pearson correlation was 0.28.

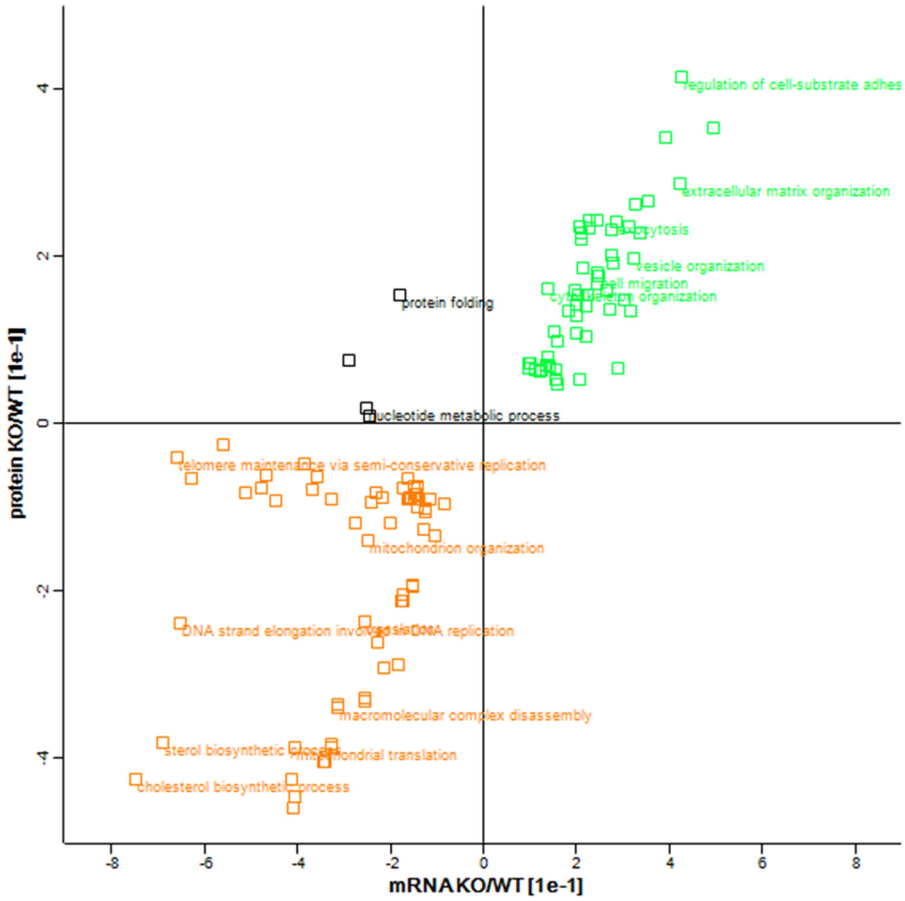

FIG. 9. **2D annotation enrichment of proteome and transcriptome expression changes.** The 2D-annotation enrichment scores for GO biological processes (GOBP names) were plotted for the proteome and transcriptome expression changes observed when comparing the MetAP1 KO *versus* WT setups. The fold change of log2 transformed means of corresponding normalized iBAQ and RPKM values were considered only in case of two valid replicate values for the proteome and transcriptome setups analyzed. The biological processes represented by green dots show common upregulation at both mRNA and protein levels, whereas orange dots indicate simultaneous downregulation or, in case of the points with low absolute Y-values, represent biological processes downregulated at the mRNA level only. The process represented by black dots exhibit downregulations at the mRNA level, while being upregulated (GOBP protein folding) or non-regulated at the level of the proteome. Only corrected *p* values <0.02 were considered.

diminish Nt-acetylation and lower iMet cleavage susceptibility (11, 49). However, because in most cases, only the steady-state levels of the main proteoforms can be detected, no general conclusions regarding the influence of iMet excision on Nt-acetylation can be drawn easily.

Interestingly, differential iMet excision did not appear to account for the differential protein expression patterns observed. On the other hand, and despite the rather moderate correlation of mRNA abundance ratios with protein abundance ratios, proteome-changes were typically reflected by altered transcript abundances.

Finally, on perturbation of MetAP activity, and besides the differential expression of proteins implicated in cell proliferation, omics expression profiling revealed differential expression of cytoskeletal proteins, proteins associated with protein and lipid and cholesterol biosynthesis. In this context, it is noteworthy that MetAP2 inhibitors, originally developed as anticancer therapies, have proven anti-obesity effects by their inhibitory action over the sterol regulatory element binding protein (SREBP), thereby resulting in reduced lipid and cholesterol biosynthesis (50). Based on our results, MetAP1 can also be put forward as a potential target for the discovery and development of new anti-obesity besides anticancer therapeutic strategies.

Acknowledgments—We thank Prof. Kris Gevaert for conceptual assistance and financial support of this research and Nucleomics Core of the VIB (Leuven) for performing the deep-sequencing experiment.

DATA AVAILABILITY

The mass spectrometry proteomics data have been deposited to the ProteomeXchange Consortium with the data set identifier PXD006638. Annotated, mass-labeled MS/MS spectra can be viewed on MS-Viewer (http:// msviewer.ucsf.edu/prospector/cgi-bin/msform.cgi?form_msviewer) (34) using the search keys umhkpodlaj (supplemental Table S2*A*), 4adxtut9up (supplemental Table S2*B*) and 7balnvbgbr (for the

33 peptides corresponding to single-peptide based protein identifications in supplemental Table S3). RNA-seq sequencing data is accessible through GEO Series accession number GSE103405 in NCBI's Gene Expression Omnibus with reviewer password: wpuxikegfnkjjkx (see also detailed description in Experimental Procedures).

* We declare no conflict of interest.

S This article contains supplemental material.

‖ To whom correspondence should be addressed: VIB-UGent Center for Medical Biotechnology, B-9000 Ghent, Belgium. Tel.: +32-92649279; Fax: +32-92649496; E-mail: Petra.VanDamme@vib-ugent.be.

¶ These authors share first authorship.

REFERENCES

1. Giglione, C., Boularot, A., and Meinnel, T. (2004) Protein N-terminal methionine excision. *Cell. Mol. Life Sci.* **61,** 1455–1474
2. Chang, S. Y., McGary, E. C., and Chang, S. (1989) Methionine aminopeptidase gene of Escherichia coli is essential for cell growth. *J. Bacteriol.* **171,** 4071–4072
3. Boxem, M., Tsai, C. W., Zhang, Y., Saito, R. M., and Liu, J. O. (2004) The C. elegans methionine aminopeptidase 2 analog map-2 is required for germ cell proliferation. *FEBS Lett.* **576,** 245–250
4. Li, X., and Chang, Y. H. (1995) Amino-terminal protein processing in Saccharomyces cerevisiae is an essential function that requires two distinct methionine aminopeptidases. *Proc. Natl. Acad. Sci. U.S.A.* **92,** 12357–12361
5. Ross, S., Giglione, C., Pierre, M., Espagne, C., and Meinnel, T. (2005) Functional and developmental impact of cytosolic protein N-terminal methionine excision in Arabidopsis. *Plant Physiol.* **137,** 623–637
6. Arfin, S. M., Kendall, R. L., Hall, L., Weaver, L. H., Stewart, A. E., Matthews, B. W., and Bradshaw, R. A. (1995) Eukaryotic methionyl aminopeptidases: two classes of cobalt-dependent enzymes. *Proc. Natl. Acad. Sci. U.S.A.* **92,** 7714–7718
7. Addlagatta, A., Hu, X., Liu, J. O., and Matthews, B. W. (2005) Structural basis for the functional differences between type I and type II human methionine aminopeptidases. *Biochemistry* **44,** 14741–14749
8. Meinnel, T., Mechulam, Y., and Blanquet, S. (1993) Methionine as translation start signal: a review of the enzymes of the pathway in Escherichia coli. *Biochimie* **75,** 1061–1075
9. Solbiati, J., Chapman-Smith, A., Miller, J. L., Miller, C. G., and Cronan, J. E., Jr. (1999) Processing of the N termini of nascent polypeptide chains requires deformylation prior to methionine removal. *J. Mol. Biol.* **290,** 607–614
10. Frottin, F., Martinez, A., Peynot, P., Mitra, S., Holz, R. C., Giglione, C., and Meinnel, T. (2006) The proteomics of N-terminal methionine cleavage. *Mol. Cell. Proteomics* **5,** 2336–2349
11. Xiao, Q., Zhang, F., Nacev, B. A., Liu, J. O., and Pei, D. (2010) Protein N-terminal processing: substrate specificity of Escherichia coli and human methionine aminopeptidases. *Biochemistry* **49,** 5588–5599
12. Arfin, S. M., and Bradshaw, R. A. (1988) Cotranslational processing and protein turnover in eukaryotic cells. *Biochemistry* **27,** 7979–7984
13. Moerschell, R. P., Hosokawa, Y., Tsunasawa, S., and Sherman, F. (1990) The specificities of yeast methionine aminopeptidase and acetylation of amino-terminal methionine in vivo. Processing of altered iso-1-cytochromes c created by oligonucleotide transformation. *J. Biol. Chem.* **265,** 19638–19643
14. Tsunasawa, S., Stewart, J. W., and Sherman, F. (1985) Amino-terminal processing of mutant forms of yeast iso-1-cytochrome c. The specificities of methionine aminopeptidase and acetyltransferase. *J. Biol. Chem.* **260,** 5382–5391
15. Bonissone, S., Gupta, N., Romine, M., Bradshaw, R. A., and Pevzner, P. A. (2013) N-terminal protein processing: a comparative proteogenomic analysis. *Mol. Cell. Proteomics* **12,** 14–28
16. Polevoda, B., and Sherman, F. (2003) N-terminal acetyltransferases and sequence requirements for N-terminal acetylation of eukaryotic proteins. *J. Mol. Biol.* **325,** 595–622
17. Arnesen, T., Van Damme, P., Polevoda, B., Helsens, K., Evjenth, R., Colaert, N., Varhaug, J. E., Vandekerckhove, J., Lillehaug, J. R., Sherman, F., and Gevaert, K. (2009) Proteomics analyses reveal the evolutionary conservation and divergence of N-terminal acetyltransferases from yeast and humans. *Proc. Natl. Acad. Sci. U.S.A.* **106,** 8157–8162
18. Brown, J. L., and Roberts, W. K. (1976) Evidence that approximately eighty per cent of the soluble proteins from Ehrlich ascites cells are Nalpha-acetylated. *J. Biol. Chem.* **251,** 1009–1014
19. Van Damme, P., Hole, K., Pimenta-Marques, A., Helsens, K., Vandekerckhove, J., Martinho, R. G., Gevaert, K., and Arnesen, T. (2011) NatF contributes to an evolutionary shift in protein N-terminal acetylation and is important for normal chromosome segregation. *PLoS Genet.* **7,** e1002169
20. Van Damme, P., Hole, K., Gevaert, K., and Arnesen, T. (2015) N-terminal acetylome analysis reveals the specificity of Naa50 (Nat5) and suggests a kinetic competition between N-terminal acetyltransferases and methionine aminopeptidases. *Proteomics* **15,** 2436–2446
21. Kim, H. K., Kim, R. R., Oh, J. H., Cho, H., Varshavsky, A., and Hwang, C. S. (2014) The N-terminal methionine of cellular proteins as a degradation signal. *Cell* **156,** 158–169
22. Gawron, D., Ndah, E., Gevaert, K., and Van Damme, P. (2016) Positional proteomics reveals differences in N-terminal proteoform stability. *Mol. Syst. Biol.* **12,** 858
23. Varshavsky, A. (2011) The N-end rule pathway and regulation by proteolysis. *Protein Sci.* **20,** 1298–1345
24. Towbin, H., Bair, K. W., DeCaprio, J. A., Eck, M. J., Kim, S., Kinder, F. R., Morollo, A., Mueller, D. R., Schindler, P., Song, H. K., van Oostrum, J., Versace, R. W., Voshol, H., Wood, J., Zabludoff, S., and Phillips, P. E. (2003) Proteomics-based target identification: bengamides as a new class of methionine aminopeptidase inhibitors. *J. Biol. Chem.* **278,** 52964–52971
25. Van Damme, P., Arnesen, T., Ruttens, B., and Gevaert, K. (2013) In-gel N-acetylation for the quantification of the degree of protein in vivo N-terminal acetylation. *Methods Mol. Biol.* **981,** 115–126
26. Staes, A., Impens, F., Van Damme, P., Ruttens, B., Goethals, M., Demol, H., Timmerman, E., Vandekerckhove, J., and Gevaert, K. (2011) Selecting protein N-terminal peptides by combined fractional diagonal chromatography. *Nat. Protocols* **6,** 1130–1141
27. Hebenstreit, D., Fang, M., Gu, M., Charoensawan, V., van Oudenaarden, A., and Teichmann, S. A. (2011) RNA sequencing reveals two major classes of gene expression levels in metazoan cells. *Mol. Syst. Biol.* **7,** 497
28. Edgar, R., Domrachev, M., and Lash, A. E. (2002) Gene Expression Omnibus: NCBI gene expression and hybridization array data repository. *Nucleic Acids Res.* **30,** 207–210
29. Stes, E., Laga, M., Walton, A., Samyn, N., Timmerman, E., De Smet, I., Goormachtig, S., and Gevaert, K. (2014) A COFRADIC protocol to study protein ubiquitination. *J. Proteome Res.* **13,** 3107–3113
30. Cox, J., and Mann, M. (2008) MaxQuant enables high peptide identification rates, individualized p.p.b.-range mass accuracies and proteome-wide protein quantification. *Nat. Biotechnol.* **26,** 1367–1372
31. Cox, J., Neuhauser, N., Michalski, A., Scheltema, R. A., Olsen, J. V., and Mann, M. (2011) Andromeda: a peptide search engine integrated into the MaxQuant environment. *J. Proteome Res.* **10,** 1794–1805
32. Cox, J., Hein, M. Y., Luber, C. A., Paron, I., Nagaraj, N., and Mann, M. (2014) Accurate proteome-wide label-free quantification by delayed normalization and maximal peptide ratio extraction, termed MaxLFQ. *Mol. Cell. Proteomics* **13,** 2513–2526
33. Vizcaino, J. A., Csordas, A., del-Toro, N., Dianes, J. A., Griss, J., Lavidas, I., Mayer, G., Perez-Riverol, Y., Reisinger, F., Ternent, T., Xu, Q. W., Wang, R., and Hermjakob, H. (2016) 2016 update of the PRIDE database and its related tools. *Nucleic Acids Res.* **44,** D447–D456
34. Baker, P. R., and Chalkley, R. J. (2014) MS-viewer: a web-based spectral viewer for proteomics results. *Mol. Cell. Proteomics* **13,** 1392–1396
35. Helsens, K., Colaert, N., Barsnes, H., Muth, T., Flikka, K., Staes, A., Timmerman, E., Wortelkamp, S., Sickmann, A., Vandekerckhove, J., Gevaert, K., and Martens, L. (2010) ms_lims, a simple yet powerful open source laboratory information management system for MS-driven proteomics. *Proteomics* **10,** 1261–1264
36. Tyanova, S., Temu, T., Sinitcyn, P., Carlson, A., Hein, M. Y., Geiger, T., Mann, M., and Cox, J. (2016) The Perseus computational platform for

comprehensive analysis of (prote)omics data. *Nat. Methods* **13,** 731–740
37. Cox, J., and Mann, M. (2012) 1D and 2D annotation enrichment: a statistical method integrating quantitative proteomics with complementary high-throughput data. *BMC Bioinformatics* **13,** S12
38. Fijalkowska, D., Verbruggen, S., Ndah, E., Jonckheere, V., Menschaert, G., and Van Damme, P. (2017) eIF1 modulates the recognition of suboptimal translation initiation sites and steers gene expression via uORFs. *Nucleic Acids Res.* **45,** 7997–8013
39. Zheng, Q., Cai, X., Tan, M. H., Schaffert, S., Arnold, C. P., Gong, X., Chen, C. Z., and Huang, S. (2014) Precise gene deletion and replacement using the CRISPR/Cas9 system in human cells. *BioTechniques* **57,** 115–124
40. Hu, X., Addlagatta, A., Lu, J., Matthews, B. W., and Liu, J. O. (2006) Elucidation of the function of type 1 human methionine aminopeptidase during cell cycle progression. *Proc. Natl. Acad. Sci. U.S.A.* **103,** 18148–18153
41. Zhang, F., Bhat, S., Gabelli, S. B., Chen, X., Miller, M. S., Nacev, B. A., Cheng, Y. L., Meyers, D. J., Tenney, K., Shim, J. S., Crews, P., Amzel, L. M., Ma, D., and Liu, J. O. (2013) Pyridinylquinazolines selectively inhibit human methionine aminopeptidase-1 in cells. *J. Medicinal Chem.* **56,** 3996–4016
42. Michalski, A., Damoc, E., Hauschild, J. P., Lange, O., Wieghaus, A., Makarov, A., Nagaraj, N., Cox, J., Mann, M., and Horning, S. (2011) Mass spectrometry-based proteomics using Q Exactive, a high-performance benchtop quadrupole Orbitrap mass spectrometer. *Mol. Cell. Proteomics* **10,** M111.011015
43. Van Damme, P., Van Damme, J., Demol, H., Staes, A., Vandekerckhove, J., and Gevaert, K. (2009) A review of COFRADIC techniques targeting protein N-terminal acetylation. *BMC Proceedings* **3,** S6
44. Van Damme, P., Gawron, D., Van Criekinge, W., and Menschaert, G. (2014) N-terminal proteomics and ribosome profiling provide a comprehensive view of the alternative translation initiation landscape in mice and men. *Mol. Cell. Proteomics* **13,** 1245–1261
45. Menschaert, G., Van Criekinge, W., Notelaers, T., Koch, A., Crappé, J., Gevaert, K., and Van Damme, P. (2013) Deep proteome coverage based on ribosome profiling aids mass spectrometry-based protein and peptide discovery and provides evidence of alternative translation products and near-cognate translation initiation events. *Mol. Cell. Proteomics* **12,** 1780–1790
46. Blomen, V. A., Majek, P., Jae, L. T., Bigenzahn, J. W., Nieuwenhuis, J., Staring, J., Sacco, R., van Diemen, F. R., Olk, N., Stukalov, A., Marceau, C., Janssen, H., Carette, J. E., Bennett, K. L., Colinge, J., Superti-Furga, G., and Brummelkamp, T. R. (2015) Gene essentiality and synthetic lethality in haploid human cells. *Science* **350,** 1092–1096
47. Frottin, F., Bienvenut, W. V., Bignon, J., Jacquet, E., Vaca Jacome, A. S., Van Dorsselaer, A., Cianferani, S., Carapito, C., Meinnel, T., and Giglione, C. (2016) MetAP1 and MetAP2 drive cell selectivity for a potent anticancer agent in synergy, by controlling glutathione redox state. *Oncotarget* **7,** 63306–63323
48. Tucker, L. A., Zhang, Q., Sheppard, G. S., Lou, P., Jiang, F., McKeegan, E., Lesniewski, R., Davidsen, S. K., Bell, R. L., and Wang, J. (2008) Ectopic expression of methionine aminopeptidase-2 causes cell transformation and stimulates proliferation. *Oncogene* **27,** 3967–3976
49. Polevoda, B., and Sherman, F. (2000) Nalpha -terminal acetylation of eukaryotic proteins. *J. Biol. Chem.* **275,** 36479–36482
50. Joharapurkar, A. A., Dhanesha, N. A., and Jain, M. R. (2014) Inhibition of the methionine aminopeptidase 2 enzyme for the treatment of obesity. *Diabetes, Metabolic Syndrome Obesity* **7,** 73–84
51. Schwanhausser, B., Busse, D., Li, N., Dittmar, G., Schuchhardt, J., Wolf, J., Chen, W., and Selbach, M. (2011) Global quantification of mammalian gene expression control. *Nature* **473,** 337–342